Supersolidity of cnoidal waves in an ultracold Bose gas

Giovanni I. Martone ◉,[1,2] Alessio Recati,[3,4] and Nicolas Pavloff ◉[1]

[1]*Université Paris-Saclay, CNRS, LPTMS, 91405 Orsay, France*
[2]*Laboratoire Kastler Brossel, Sorbonne Université, CNRS, ENS-Université PSL, Collège de France, 4 Place Jussieu, 75005 Paris, France*
[3]*INO-CNR BEC Center and Dipartimento di Fisica, Università di Trento, 38123 Povo, Italy*
[4]*Trento Institute for Fundamental Physics and Applications, INFN, 38123 Trento, Italy*

A one-dimensional Bose-Einstein condensate may experience nonlinear periodic modulations known as cnoidal waves. We argue that such structures represent promising candidates for the study of supersolidity-related phenomena in a nonequilibrium state. A mean-field treatment makes it possible to rederive Leggett's formula for the superfluid fraction of the system and to estimate it analytically. We determine the excitation spectrum, for which we obtain analytical results in the two opposite limiting cases of (i) a linearly modulated background and (ii) a train of dark solitons. The presence of two Goldstone (gapless) modes, associated with the spontaneous breaking of U(1) symmetry and of continuous translational invariance, at long wavelength is verified. We also calculate the static structure factor and the compressibility of cnoidal waves, which show a divergent behavior at the edges of each Brillouin zone.

I. INTRODUCTION

Supersolid phases of matter have attracted increasing interest in the past few years. In these configurations two apparently conflicting properties, namely, superfluidity and crystalline order, can coexist, giving rise to novel features (see, for instance, the reviews in [1–4]). The existence of such a phenomenon had initially been investigated, and apparently ruled out, by Penrose and Onsager [5]. It was reproposed shortly thereafter by Gross. In Refs. [6,7] he considered a system of interacting bosons in the semiclassical limit, where the bosonic quantum field can be replaced by a classical one, which obeys a nonlinear field equation. The latter admits periodic solutions, describing a uniform background with a crystal lattice on top of it. In the subsequent decades the search for possible superfluid solid phases was extended and other scenarios in which supersolidity could occur were examined [8–14]. The main candidate has been for many years the solid phase of helium. However, the most recent experimental results and theoretical analyses seem to preclude superfluidity in bulk solid helium [1], and the attention turned to solid-helium two-dimensional films [15].

On the other hand, significant progress has been made recently with ultracold atomic gases, with the first observations of an incompressible supersolid state in bosonic systems coupled to two optical cavities [16] and of a superfluid smectic state in spin-orbit-coupled Bose-Einstein condensates [17].

Even more recently, coherent droplet arrays have been realized in dipolar quantum gases [18–20]. This has stimulated a large amount of further experimental work, shedding light on the spectrum and the collective modes [21–24], the superfluidity properties [25], and the out-of-equilibrium dynamics [26] of this exotic phase of matter.

A rather intriguing scenario for the occurrence of supersolidity is the one pointed out by Pitaevskii in [13]. He proved that a sample of superfluid ^{4}He flowing along a capillary with a velocity exceeding Landau's critical value develops a layered structure. This structure results from the condensation of excitations close to the roton momentum [27] and is at rest with respect to the walls of the capillary. Its excitation spectrum is deformed such that the system remains superfluid. These findings were later confirmed by numerical simulations based on a density functional approach [28]. The same physics can be observed in ultracold Bose gases as well, as found by Baym and Pethick [29]. In this reference the authors assumed a finite-range interaction between particles. This shifts the critical momentum at which the Landau instability can occur to a finite value. Similar to ^{4}He, a large number of excitations with momentum close to this value (called levons) are created when crossing the Landau velocity, which represents the onset of the transition to the layered phase. The latter features a superfluid fraction smaller than 1.

In general, supersolidlike configurations can have lower energy than uniform ones only in special circumstances. Typically one needs to have either specific kinds of interparticle interactions (such as dipole-dipole, finite-range, or cavity-mediated) or a properly modified single-particle spectrum (as in the case of spin-orbit-coupled Bose-Einstein condensates). However, when none of these conditions is fulfilled, one may still have a supersolid behavior in some excited state. This is the case of a standard quasi-one-dimensional dilute Bose

gas with repulsive contact interaction, which is described by the Gross-Pitaevskii equation. This equation is known to have spatially periodic stationary solutions, which were studied by Tsuzuki in [30]. Korteweg and de Vries [31] had coined the term "cnoidal waves" for solutions of this type, because they can be expressed in terms of the Jacobi cosine amplitude function, denoted by cn [32]. In systems of bosons rotating in a ring trap, transitions between metastable uniform and cnoidal configurations have been predicted [33,34]. Very recently, cnoidal-wave-like solutions have been found for the extended Gross-Pitaevskii equation describing a self-trapped cigar-shaped Bose gas [35].

Cnoidal waves can be regarded as the equivalent of Pitaevskii's layered phase for an ultracold Bose gas. At variance with the case considered in Ref. [29], for a repulsive contact interaction the Landau instability takes place at vanishing momentum and there is no mechanism similar to levon condensation. Nevertheless, one can achieve a cnoidal structure by moving an obstacle at a suitable velocity through the condensate. The scope of this work is to highlight that these configurations exhibit typical features of supersolids in both their static and dynamic behavior. As such, they are candidates for studying phenomena related to supersolidity within the most standard Bose-Einstein condensates. The latter do not suffer from the strong three-body losses typical of dilute ultracold systems in which the stabilization is due to beyond-mean-field equation of states, as for dipolar gases and quantum mixtures.

This article is organized as follows. In Sec. II we introduce the model to investigate and the equations governing it. In Sec. III we present the derivation of the cnoidal-wave solution and illustrate some of its most important properties. The dynamic behavior of a cnoidal wave is discussed in Sec. IV, where we discuss the excitation spectrum, the static structure factor, and the compressibility. We summarize in Sec. V. Finally, some technical details are presented in the Appendixes: Appendix A presents the properties of the cnoidal wave in some limiting cases, the procedure for solving the Bogoliubov equations is explained in Appendix B, and Appendix C computes the lower branch of the spectrum of a train of dark solitons.

II. MODEL

Let us consider a quasi-one-dimensional weakly interacting Bose-Einstein condensate at zero temperature. The condensate wave function $\psi(x, t)$ obeys the Gross-Pitaevskii equation

$$i\hbar\psi_t = -\frac{\hbar^2}{2m}\psi_{xx} + (g|\psi|^2 - \mu)\psi. \tag{1}$$

Here m is the mass of a particle, $g > 0$ the interaction strength, and μ the chemical potential. We use in Eq. (1) and throughout the paper the convention that subscripts denote derivatives with respect to x and t.

Equation (1) is a one-dimensional (1D) classical field equation which is valid in the so-called 1D mean-field regime [36]. For a condensate transversely confined by a harmonic trap of angular frequency $\omega_\perp$, this regime is defined by the inequalities

$$\left(\frac{a}{a_\perp}\right)^2 \ll n_{1D}a \ll 1, \tag{2}$$

where a is the s-wave scattering length, $a_\perp = \sqrt{\hbar/m\omega_\perp}$ is the transverse harmonic-oscillator length, and n_{1D} is a typical order of magnitude of the linear atom density $n = |\psi|^2$. In this regime one has $g = 2\hbar\omega_\perp a$ [37]. For a transverse trap of angular frequency $\omega_\perp = 1$ kHz, one gets $(a_\perp/a)^2 = 1.7 \times 10^{-5}$ for ^{23}Na and $(a_\perp/a)^2 = 2.6 \times 10^{-4}$ for ^{87}Rb, which means that the 1D mean-field regime where Eq. (1) is valid ranges over about four orders of magnitude in density.

We now perform a Madelung transform, which amounts to writing the wave function in the form $\psi = Ae^{i\Theta}$. Inserting this expression into the Gross-Pitaevskii equation (1) yields two coupled equations for the real quantities $A \geqslant 0$ and Θ. The first one, expressing the particle number conservation, is the continuity equation, which reads

$$n_t + \left(\frac{\hbar\Theta_x}{m}n\right)_x = 0, \tag{3}$$

where we recall that $n = A^2$ is the linear density and $v = \hbar\Theta_x/m$ the velocity field. The second Madelung equation reads

$$\hbar\Theta_t = \frac{\hbar^2}{2m}\frac{A_{xx}}{A} - \frac{m}{2}\left(\frac{\hbar\Theta_x}{m}\right)^2 - gA^2 + \mu. \tag{4}$$

After taking the gradient on both sides, it becomes formally identical to the Euler equation for the potential flow of an inviscid fluid, with the addition of a quantum potential.

III. CNOIDAL-WAVE SOLUTION

The cnoidal-wave solution exhibited by the Gross-Pitaevskii equation (1) has been extensively studied in the literature. In this section we review its derivation in order to fix the notation and set the background for the subsequent calculations. Then we present some of its most relevant features and in particular we derive an analytic expression for the superfluid density.

A. Derivation of the cnoidal-wave solution

In order to find stationary solutions of the Gross-Pitaevskii equation (1) one has to set $n_t = 0$ and $\Theta_t = 0$. This turns Eqs. (3) and (4) into ordinary differential equations in x. Following Ref. [30], we will integrate these equations by imposing the condition that the condensate density and velocity oscillate in space at a given wavelength Λ around fixed average values $\bar{n}$ and $\bar{v}$. Integrating once Eq. (3) with respect to x, one obtains

$$\Theta_x = \frac{m\mathcal{J}}{\hbar n}, \tag{5}$$

where $\mathcal{J}$ denotes the constant value of the current density. We can use this result to eliminate Θ_x from Eq. (4). This yields
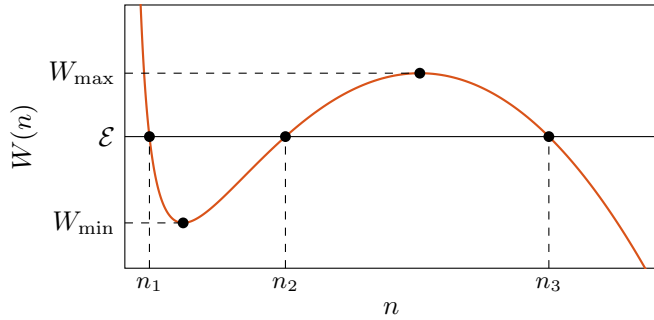
$$\frac{\hbar^2}{2m}A_x^2 + W(n) = \mathcal{E}, \tag{6}$$

FIG. 1. Schematic behavior of the potential W as a function of n. The value of W at the local minimum (maximum) is $W_{\min}$ ($W_{\max}$). Here $n_1 \leqslant n_2 \leqslant n_3$ are the roots of $W(n) = \mathcal{E}$.

where

$$W(n) = \frac{m\mathcal{J}^2}{2n} - \frac{gn^2}{2} + \mu n. \qquad (7)$$

Equation (6) has the same mathematical structure as the energy conservation of a classical particle having position A at time x [38,39]. The integration constant $\mathcal{E}$ plays the role of the energy and W that of the external potential. In the following we assume that the current $\mathcal{J}$ verifies the inequality [40,41]

$$\mathcal{J}^2 < \frac{8\mu^3}{27mg^2}, \qquad (8)$$

which ensures that $W(n > 0)$ has a local minimum $W_{\min}$ and a local maximum $W_{\max}$, as illustrated in Fig. 1. The maximal value (8) of $\mathcal{J}$ is analogous to the Ginzburg-Landau critical current in a superconductor [42].

For given values of the parameters, the range of values that the solutions of Eq. (6) can take is fixed by the condition $W(n) \leqslant \mathcal{E}$. In particular, the roots of $W(n) = \mathcal{E}$ identify the extrema of n, where $A_x = 0$. They are the analogous to the turning points of a classical system. In the case $W_{\min} < \mathcal{E} < W_{\max}$ considered in Fig. 1 there are three such roots, which we denote by n_1, n_2, and n_3, with $0 \leqslant n_1 \leqslant n_2 \leqslant n_3$. Let us then rewrite Eq. (6) as

$$\left(\frac{n_x}{2}\right)^2 = \frac{mg}{\hbar^2}\left(n^3 - \frac{2\mu}{g}n^2 + \frac{2\mathcal{E}}{g}n - \frac{m\mathcal{J}^2}{g}\right)$$
$$= \frac{mg}{\hbar^2}(n - n_1)(n - n_2)(n - n_3). \qquad (9)$$

Comparing the two lines of Eq. (9), one immediately finds out how to express μ, $\mathcal{E}$, and $\mathcal{J}$ in terms of n_1, n_2, and n_3. The result reads

$$\mu = \frac{g(n_1 + n_2 + n_3)}{2}, \qquad (10a)$$

$$\mathcal{E} = \frac{g(n_1 n_2 + n_2 n_3 + n_3 n_1)}{2}, \qquad (10b)$$

$$\mathcal{J}^2 = \frac{gn_1 n_2 n_3}{m}. \qquad (10c)$$

A bounded solution of Eq. (9) oscillates between n_1 and n_2 and thus is of the form

$$n(x) = n_1 \cos^2 \varphi(x) + n_2 \sin^2 \varphi(x). \qquad (11)$$

Inserting this ansatz into Eq. (9) yields (upon properly defining the spatial origin)

$$\varphi(x) = \mathrm{am}\left(\frac{\sqrt{mg(n_3 - n_1)}}{\hbar}x \Big| m_e\right), \qquad (12)$$

where am is Jacobi's amplitude function [32] and

$$m_e = \frac{n_2 - n_1}{n_3 - n_1} \in [0, 1]. \qquad (13)$$

The corresponding density and phase read

$$n(x) = n_1 + (n_2 - n_1)\mathrm{sn}^2\left(\frac{\sqrt{mg(n_3 - n_1)}}{\hbar}x \Big| m_e\right), \qquad (14)$$

$$\Theta(x) = \pm\sqrt{\frac{n_2 n_3}{n_1(n_3 - n_1)}}\Pi(-n_e; \varphi(x)|m_e). \qquad (15)$$

Here $\mathrm{sn}(u|m_e) = \sin[\mathrm{am}(u|m_e)]$ is the Jacobi sine amplitude function and $\Pi(-n_e; \varphi|m_e)$ denotes the incomplete elliptic integral of the third kind [32]. The quantity $-n_e = -(n_2 - n_1)/n_1$ is called the characteristic. The condensate phase (15) was determined by integrating Eq. (5) with respect to x, imposing $\Theta(0) = 0$ for simplicity; the plus (minus) sign corresponds to a positive (negative) value of the current $\mathcal{J}$.

Equations (14) and (15) express the cnoidal-wave solution of the Gross-Pitaevskii equation (1). It was first investigated by Tsuzuki in Ref. [30] (see also Ref. [43]). This solution depends on the three parameters $n_1 \leqslant n_2 \leqslant n_3$. It represents a stationary layered structure, i.e., such that its density profile exhibits periodic spatial modulations; a fixed current $\mathcal{J}$ flows through the fringes. The oscillation wavelength and average density are computed in Sec. III B below and are given by Eqs. (16) and (17), respectively. The modulations correspond to a spontaneous breaking of continuous translational invariance. Because of the simultaneous presence of superfluid and crystal order, cnoidal waves are expected to exhibit a supersolid behavior in both their static and dynamic properties. These aspects will be elucidated in the following sections.

B. Properties of the cnoidal-wave solution

We will now examine some characteristic features of cnoidal waves. These include the average density, the contrast of the density modulations, the superfluid fraction, and the energy per particle.

1. Density profile and contrast of the fringes

The density profile (14) oscillates with a wavelength

$$\Lambda = \frac{2K(m_e)\hbar}{\sqrt{mg(n_3 - n_1)}}, \qquad (16)$$

where $K(m_e)$ is the complete elliptic integral of the first kind [32]. These oscillations occur around an average value given by [30]

$$\bar{n} = \frac{1}{\Lambda}\int_{-\Lambda/2}^{\Lambda/2} dx\, n(x) = n_1 + (n_3 - n_1)\left[1 - \frac{E(m_e)}{K(m_e)}\right], \qquad (17)$$

where $E(m_e)$ is the complete elliptic integral of the second kind [32]. Using this average density, we can define the healing length $\xi = \hbar/\sqrt{mg\bar{n}}$ and the sound velocity $c = \sqrt{g\bar{n}/m}$.
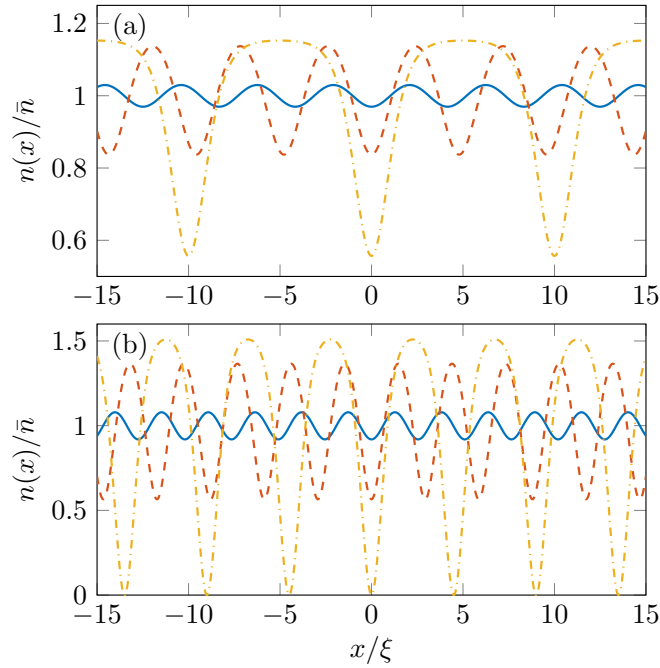
FIG. 2. Density profiles $n(x)$ of cnoidal waves for (a) $\eta = 0.6$ and (b) $\eta = 1.6$ and for $m_e = 0.1$ (blue solid lines) and $m_e = 0.5$ (red dashed lines). The value of m_e for the two yellow dash-dotted curves was chosen so as to minimize the superfluid density (23) [see also the red dashed lines of Figs. 3(c) and 3(d)]. It is equal to 0.993 in (a) and to $m_e^{\max} = 0.943$ in (b).
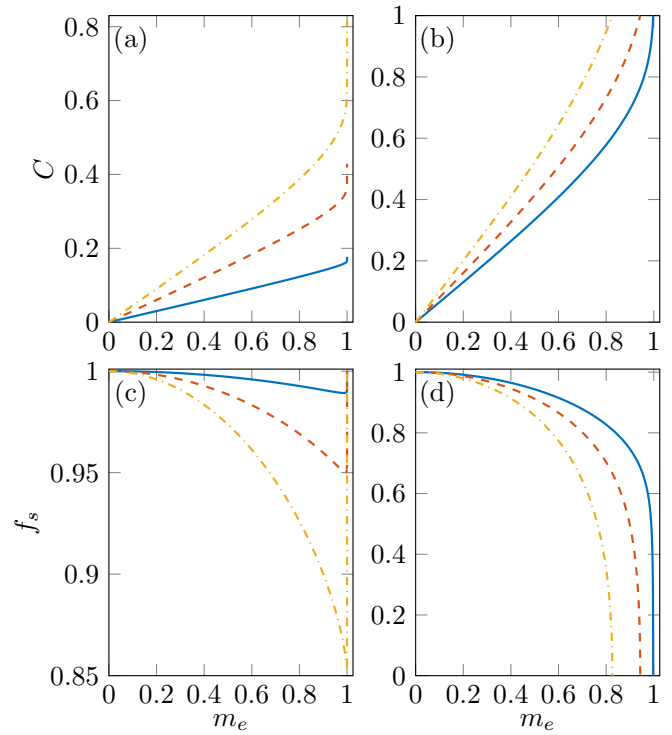

FIG. 3. (a) and (b) contrast of the fringes and (c) and (d) corresponding superfluid density as functions of m_e for (a) and (c) $\eta = 0.3$ (blue solid line), 0.6 (red dashed line), and 0.9 (yellow dash-dotted line) and (b) and (d) $\eta = 1.3$ (blue solid line), 1.6 (red dashed line), and 2.0 (yellow dash-dotted line). For the curves in (b) and (d) the corresponding values of $m_e^{\max}$ are 0.997, 0.943, and 0.826, respectively.

It is useful to rewrite n_1, n_2, and n_3 in terms of $\bar{n}$ and of the two dimensionless parameters m_e and

$$\eta = \frac{n_3 - n_1}{\bar{n}}. \tag{18}$$

From Eqs. (13) and (17) one gets

$$\frac{n_1}{\bar{n}} = 1 - \eta[1 - \Gamma(m_e)], \tag{19a}$$

$$\frac{n_2}{\bar{n}} = 1 + \eta[\Gamma(m_e) + m_e - 1], \tag{19b}$$

$$\frac{n_3}{\bar{n}} = 1 + \eta\Gamma(m_e), \tag{19c}$$

where $\Gamma(m_e) = E(m_e)/K(m_e)$. One can easily check that the conditions $0 \leqslant m_e \leqslant 1$ and $\eta \geqslant 0$ are sufficient to ensure that n_2 and n_3 are non-negative. Additional constraints come from the requirement $n_1 \geqslant 0$. The latter is satisfied for any $0 \leqslant m_e \leqslant 1$ if $0 \leqslant \eta \leqslant 1$, but if $\eta > 1$, m_e should not be larger than a threshold value $m_e^{\max}$ defined by $\Gamma(m_e^{\max}) = (\eta - 1)/\eta$. In the following we will see that, when considered as functions of m_e, the various observables have different behaviors, depending on whether η is smaller or larger than 1.

Making use of the average density (17), we can decompose the density (14) into a uniform and a modulated component as $n(x) = \bar{n} + \Delta n(x)$, with

$$\Delta n(x) = \bar{n}\eta\left[m_e \mathrm{sn}^2\left(\sqrt{\eta}\frac{x}{\xi}\bigg|m_e\right) + \Gamma(m_e) - 1\right]. \tag{20}$$

In Fig. 2 we report a few density profiles of cnoidal waves for different values of m_e and η. At small m_e the oscillations have

small amplitude and are practically sinusoidal, as discussed in Appendix A 2. Increasing m_e at fixed η produces fringes with larger amplitude and wavelength, as well as significant deviations from the sinusoidal behavior. When m_e is close to 1 the density profile takes the characteristic shape of a soliton train, made by quasiuniform regions separated by thin deep valleys.

A useful quantity to characterize the fringes is their contrast,

$$C = \frac{n_2 - n_1}{n_2 + n_1} = \frac{m_e}{m_e + 2\Gamma(m_e) - 2(\eta - 1)/\eta}. \tag{21}$$

At small m_e the contrast behaves like $C \simeq m_e\eta/2$, whereas beyond this regime two cases should be distinguished. When $\eta \leqslant 1$ the parameter m_e can vary between 0 and 1, the two extreme values corresponding to a uniform and a dark-soliton configuration, respectively (see Appendix A). Consequently, the contrast smoothly increases from 0 to a value $\eta/(2 - \eta) \leqslant 1$ at increasing m_e [see Fig. 3(a)]. In particular for $m_e = \eta = 1$, which corresponds to a black soliton, one has $C = 1$. The situation is different for $\eta > 1$, where m_e can only vary in a smaller range of values, as discussed earlier. As shown in Fig. 3(b), in this case the contrast always reaches its maximum value $C = 1$ at $m_e = m_e^{\max}$, and thus one can have density fringes oscillating between 0 and $\eta m_e^{\max}\bar{n}$ [see the yellow dash-dotted curve of Fig. 2(b)].

2. Average velocity and superfluid fraction

The velocity field $v = \hbar \Theta_x / m$ oscillates with the same wavelength Λ as the density. Its average value is

$$\bar{v} = \frac{1}{\Lambda} \int_{-\Lambda/2}^{\Lambda/2} dx \, v(x) = \frac{\mathcal{J}}{f_s \bar{n}}, \tag{22}$$

where we define

$$f_s = \left[\frac{\bar{n}}{\Lambda} \int_{-\Lambda/2}^{\Lambda/2} \frac{dx}{n(x)} \right]^{-1}$$
$$= \frac{1 - \eta[1 - \Gamma(m_e)]}{\Pi(-n_e | m_e)} K(m_e), \tag{23}$$

with $\Pi(-n_e | m_e) = \Pi(-n_e; \pi/2 | m_e)$ the complete elliptic integral of the third kind [32]. Note that Eq. (22) can be rewritten in the natural form

$$\mathcal{J} = f_s \bar{n} \bar{v}, \tag{24}$$

which indicates that f_s is precisely the superfluid fraction of the system [44]. Our first equality in Eq. (23) coincides indeed with the well-known estimate of the superfluid fraction for a supersolid introduced by Leggett [11,45]. Actually, in these works the first line of Eq. (23) was shown to be an upper bound to the real superfluid fraction. It was derived using an ansatz wave function that assumes all the particles in the superfluid to have the same phase. This assumption is weaker than the one we make in the present work using the Gross-Pitaevskii theory, in which all the atoms have the same wave function. This is why within this approximation Eq. (23) is found as an exact result.

Equations (22)–(24) constitute one of the important results of the present work, where Leggett's formula for f_s comes out as an immediate consequence of the definition of the average condensate velocity, allowing us to provide also an analytical expression for f_s. It is worth investigating the behavior of f_s as a function of the parameters characterizing the cnoidal-wave solution. The strength of f_s as a function of m_e and for different values of η is reported in Figs. 3(c) and 3(d). At fixed η and small m_e, where cnoidal waves reduce to Bogoliubov oscillations (see Appendix A 2), the superfluid fraction retains the trivial value $f_s = 1$. Expanding Eq. (23) up to second order in m_e so as to take the first nonlinear correction into account, one finds $f_s \simeq 1 - \eta^2 m_e^2/8 = 1 - C^2/2$. This result matches very well the curves in Figs. 3(c) and 3(d) at small m_e (an analogous relation was recently derived in Ref. [46] for a shallow sine-modulated supersolid). For $\eta < 1$ [Fig. 3(c)] f_s decreases at increasing m_e down to a minimum that is typically attained at some m_e very close to 1; then it undergoes a smooth but very steep ascent and goes back to 1 at $m_e = 1$, where the cnoidal wave turns into a dark soliton (see Appendix A 3). Instead, when $\eta = 1$ the superfluid density continues to drop down to 0 as m_e approaches 1. In the $\eta > 1$ regime [Fig. 3(d)], also, f_s monotonically decreases with m_e from 1 to 0, the latter value being attained at $m_e = m_e^{\max}$, where the contrast of the fringes (21) is 1. Thus a cnoidal wave with strong modulations is very weakly superfluid, again in agreement with Leggett's arguments [11,45].

On the theoretical side, the situation encountered here is common also to the modulated configurations studied for dipolar Bose gases. Leggett's equation coincides with the superfluid density obtained from single-orbital density functional theory, also known as the extended Gross-Pitaevskii equation, and it becomes zero when the periodic structure has contrast $C = 1$ (see, e.g., Refs. [46–48]). Although a number of properties have been experimentally measured, the smallness of the sample and its short lifetime have precluded direct access to the superfluid density so far (see, however, Ref. [25] for an attempt in this direction).

Let us also mention that in the stripe phase of spin-orbit-coupled Bose gases the maximum achievable value of the contrast depends on the interaction strength in the various spin channels and the deeply modulated regime with a small superfluid fraction is more challenging to reach [49].

3. Energy per particle

The energy per particle is given by

$$\varepsilon = N_\Lambda^{-1} \int_{-\Lambda/2}^{\Lambda/2} dx \left[\frac{\hbar^2 A_x^2}{2m} + \frac{mn}{2} \left(\frac{\hbar \Theta_x}{m} \right)^2 + \frac{gn^2}{2} \right], \tag{25}$$

where the prefactor accounts for the number of particles in each layer, $N_\Lambda = \bar{n}\Lambda$. The evaluation of the integral in the expression (25) can be simplified using Eqs. (5), (6), (10), and (19). The final result is

$$\frac{\varepsilon}{g\bar{n}} = 1 + \frac{\eta}{2}[3\Gamma(m_e) + m_e - 2]$$
$$+ \frac{\eta^2}{6}[3\Gamma^2(m_e) - 2(2 - m_e)\Gamma(m_e) + 1 - m_e]. \tag{26}$$

We have checked that the minimization of ε with respect to m_e and η at fixed average density $\bar{n}$ and velocity $|\bar{v}| > c$ always gives a uniform state. Hence, unlike in the case of superfluid helium [13] and of Bose gases with finite-range interaction [29], here there is no spontaneous transition from a uniform to a layered structure when the fluid velocity crosses the critical one (equal to c in our case). For this reason, cnoidal waves should be regarded as (nonlinear) excited states of the system.

IV. DYNAMIC PROPERTIES

This section is devoted to the study of the quantities characterizing the dynamic behavior of a cnoidal wave. We first derive the Bogoliubov equations (Sec. IV A). Then, in Sec. IV B, we compute and discuss the excitation spectrum, whereas in Sec. IV C we study the dynamic structure factor, its moments, and the sum rules they obey. We note here that the spectrum of cnoidal waves has been studied by the mathematical physics community (see, e.g., Refs. [50–53] and references therein), which mainly addressed the problem of dynamic stability; our focus is different and concerns the energetic instability on one side and the relationship with the phenomenon of supersolidity on the other side.

A. Bogoliubov equations

We will now use the Bogoliubov approach [54–56] to study small oscillations about the equilibrium configuration derived in Sec. III A. In the present context it is convenient to describe the collective modes in terms of the fluctuations of the density and the phase. To this aim we decompose the total density and

phase as $n(x) + \delta n(x, t)$ and $\Theta(x) + \delta\Theta(x, t)$, respectively. At first order in δn and $\delta\Theta$ Eqs. (3) and (4) become

$$\delta n_t = -\frac{\hbar}{m}(\Theta_x \delta n_x + \Theta_{xx} \delta n + n \delta\Theta_{xx} + n_x \delta\Theta_x), \quad (27a)$$

$$\delta\Theta_t = \frac{\hbar}{4m}\left(\frac{\delta n_{xx}}{n} - \frac{n_x}{n^2}\delta n_x + \frac{n_x^2 - n n_{xx}}{n^3}\delta n\right)$$
$$- \frac{\hbar\Theta_x}{m}\delta\Theta_x - \frac{g}{\hbar}\delta n. \quad (27b)$$

We look for solutions oscillating in time of the form

$$\delta n(x, t) = \delta\tilde{n}(x)e^{-i\omega t} + \delta\tilde{n}^*(x)e^{i\omega t}, \quad (28a)$$

$$\delta\Theta(x, t) = \delta\tilde{\Theta}(x)e^{-i\omega t} + \delta\tilde{\Theta}^*(x)e^{i\omega t}. \quad (28b)$$

This turns Eqs. (27) into an eigenvalue problem, which enables one to determine the frequency ω and the complex amplitudes $\delta\tilde{n}$ and $\delta\tilde{\Theta}$. The latter obey the normalization condition [56]

$$i\int_{-\Lambda/2}^{\Lambda/2} dx[\delta\tilde{n}^*(x)\delta\tilde{\Theta}(x) - \delta\tilde{\Theta}^*(x)\delta\tilde{n}(x)] = 1. \quad (29)$$

For each solution $\delta\tilde{n}$ and $\delta\tilde{\Theta}$ with frequency ω there exists another one, $\delta\tilde{n}^*$ and $\delta\tilde{\Theta}^*$, having frequency $-\omega$ [54]. The integral of Eq. (29) evaluates to -1 (instead of 1) for the latter solution. Both solutions correspond to the same physical oscillation, as clear from the structure of Eqs. (28). In order to avoid this redundancy we will only consider solutions having positive norm. This choice is customary because, in a second-quantization framework, it is naturally associated with the usual boson commutation relation.

B. Excitation spectrum

The procedure for solving this eigenvalue problem is similar to that employed in the previous works [57,58] and is detailed in Appendix B. Since the coefficients of the linear coupled equations (27) are periodic in x, we can look for solutions $\delta\tilde{n}$ and $\delta\tilde{\Theta}$ in the form of Bloch waves [59]. They are given by a plane wave, with wave vector q, times a periodic function with period Λ [see Eqs. (B3)]. To any fixed value of q there correspond infinitely many solutions, with different amplitudes and frequencies. This is at the origin of the band structure exhibited by the Bogoliubov spectrum. This structure is clearly visible in Fig. 4, where we plot the lowest three bands of the spectrum of elementary excitations of two given cnoidal-wave solutions. To distinguish between the various Bogoliubov modes we make use of two subscripts, the quasimomentum q and the band index $\ell = 1, 2, \ldots$. The spectrum is periodic in q, with period $Q = 2\pi/\Lambda$ equal to the wave vector of the density modulations. Each range of values of q enclosed between consecutive integer multiples of Q defines a Brillouin zone. Notice that the frequencies $\omega_{\ell,q}$ are not invariant under inversion of q into $-q$; this reflects the fact that cnoidal-wave solutions do not enjoy parity and time-reversal symmetry separately when the current $\mathcal{J}$ they carry is not zero. For the sake of comparison, in each panel of Fig. 4 we also plot (dashed curve) the spectrum of a uniform Bose gas having the same average density $\bar{n}$ and velocity $\bar{v}$ as the cnoidal wave considered in the panel.
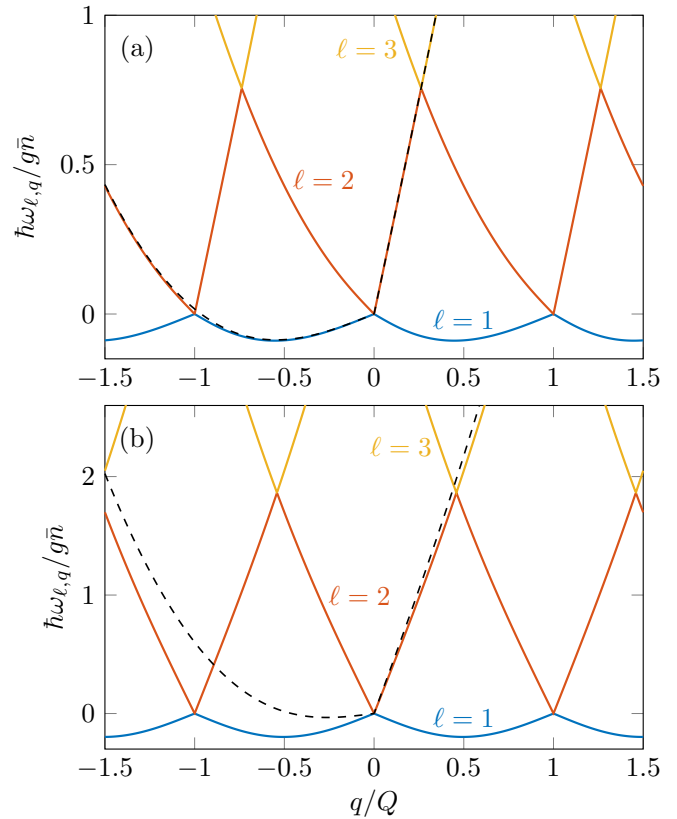

FIG. 4. Lowest three bands of the excitation spectrum as functions of q for (a) the same parameters $\eta = 0.6$ and $m_e = 0.5$ as the red dashed curve of Fig. 2(a) and (b) $\eta = 2.0$ and a value $m_e = 0.8$ very close to $m_e^{max} = 0.826$ [see yellow dash-dotted curves of Figs. 3(b) and 3(d)]. In both cases the sign of the current density $\mathcal{J}$ is taken to be positive. The black dashed lines show the spectrum of a uniform system having the same average density $\bar{n}$ and velocity (a) $\bar{v}/c = 1.18$ and (b) $\bar{v}/c = 1.10$ as the cnoidal waves under consideration.

The main feature of the spectra of Fig. 4 is that the two lowest bands ($\ell = 1, 2$) are gapless and have linear dispersion close to the edges of each Brillouin zone. The higher branch ($\ell = 2$) at small positive q and the lower one ($\ell = 1$) at negative q are already present in a uniform system (dashed curve), whereas the other two branches are specific of cnoidal waves.[1]

The presence of two gapless Goldstone modes is a feature expected for the spectrum of a one-dimensional supersolid intended as a system which breaks both U(1) and continuous translational invariance (see, e.g., Ref. [60] for a detailed discussion). Such an increase of gapless modes has indeed been discussed theoretically for the supersolid phase of solid helium [9], of soft-core Bose gases [61–64], and of dipolar Bose gases, as well as for the stripe phase in spin-orbit-coupled Bose gases [57,65]. It is under very active experimental investigation for dipolar gases [21–24].

The two gapless bands of Fig. 4, as well as all the upper bands of the excitation spectrum, have real frequency. This result confirms that cnoidal waves in one-dimensional

---

[1]This actually holds only for positive $\bar{v}$; the situation is reversed when $\bar{v} < 0$.

Bose gases with repulsive contact interaction are dynamically stable, as pointed out in Refs. [50–53]. However, different from other supersolids considered in the literature, here the frequency of the lowest gapless band is negative, meaning that these waves are energetically unstable. This agrees with the fact that they are excited states of the system, as discussed in Sec. III B 3.[2] Such an instability can lead to the decay of a cnoidal wave to a lower-energy state if one applies an external perturbation. However, if this decay takes place over sufficiently long timescales, measurements of the dispersion relation based on Bragg spectroscopy techniques would still be feasible. It is worth mentioning that the situation is not very different from that of dipolar gases. Indeed, due to three-body losses (energetic instability), the lifetime of the supersolid phase in those systems is very short (few to tens milliseconds) but many measurements, from phase coherence to collective excitations to Bragg spectroscopy, have been performed [18–26], aiming at confirming the supersolid behavior. This phenomenon can be referred to as transient supersolidity.

A practical consequence of the structure of the excitation spectrum we just discussed is that our system cannot flow around an external obstacle without dissipating energy. It is well known that for nonuniform systems (such as Bose-Einstein condensates in optical lattices and supersolids) the question of drag in the presence of an external obstacle is a different issue from superfluidity. The latter corresponds to a dissipationless flow of particles of the fluid through the fluid itself [44] (see also the discussion in Sec. I B of Ref. [2]), evidenced by the existence of a finite superfluid fraction, which for cnoidal waves is given by Eq. (23). The occurrence of drag in a supersolid flowing past an external body was first pointed out by Pomeau and Rica in Ref. [14]. Subsequently, Ref. [58] computed the drag force experienced by a spin-orbit-coupled Bose-Einstein condensate in the supersolid stripe phase moving through a pointlike impurity, showing that energy dissipation occurs at any condensate speed. In these examples drag occurs because the lowest-lying bands of the Bogoliubov spectrum have vanishing frequency at the edges of each Brillouin zone, yielding a zero Landau critical velocity. In the case of cnoidal waves, the energetic instability can make the effects of the drag more dramatic because the interaction with an external body can populate the negative-frequency modes.

The nature of the two gapless bands can be understood by looking at the limit where their frequencies vanish. This happens when q lies on an edge of a Brillouin zone. Setting $\delta n_t = 0$ and $\delta \Theta_t = 0$ in Eqs. (27), one finds two kinds of solutions. The first one is $\delta n = 0$ and $\delta \Theta$ equal to a constant; it corresponds to an infinitesimal U(1) transformation of the phase of the condensate wave function. The second solution is $\delta n = n_x \delta x_0$ and $\delta \Theta = \Theta_x \delta x_0$, which performs a translation of the wave function by an infinitesimal displacement δx_0. This finding further reinforces the idea that the appearance of these modes is a result of the spontaneous breaking of U(1) and continuous translational symmetry.

For modes with nonzero frequency one can still distinguish between a crystal and phase character. The former involves small oscillations of the density peaks about their equilibrium positions; the latter features a superfluid current of particles tunneling from one peak to another [21,23,62,64]. However, hybridization can occur and both characters can be present in a single mode when $\omega_{\ell,q} \neq 0$. In cnoidal waves with small m_e, the $\ell = 1$ branch at $q \lesssim 0$ and the $\ell = 2$ one at $q \gtrsim 0$ have a dominant phase character, which is explained by their closeness to the corresponding modes of a uniform gas [dashed curve of Fig. 4(a)]; conversely, the branches that do not appear in uniform systems are mainly crystal modes. This change of behavior when crossing $q = 0$ becomes less and less pronounced at increasing m_e because of stronger hybridization. When m_e is large [close to 1 for $\eta \lesssim 1$ and to $m_e^{\max}$ for $\eta > 1$, as in Fig. 4(b)] we find that the $\ell = 1$ branch becomes dominantly crystal-like for both positive and negative q. In particular, in the $\eta \lesssim 1$ and $m_e \lesssim 1$ case the frequency of this band is almost 0 at all q, and in the $m_e \to 1$ limit it reduces to the zero-frequency mode of the excitation spectrum of a dark soliton. For $\eta > 1$ and m_e close to $m_e^{\max}$ the phase character of both gapless bands is further suppressed because of the strong reduction of the superfluid fraction pointed out in Sec. III B 2.

As we mentioned in Sec. III B 1, at $\eta \lesssim 1$, m_e can reach values close to unity, and in this regime cnoidal waves can be regarded as chains of dark solitons. It is proven in Appendix C that in this case the dispersion relation of the lowest band has the following analytic expression:

$$\frac{\hbar \omega_{1,q}}{g\bar{n}} = -8\eta^{3/2} e^{-\sqrt{\eta}\Lambda/\xi} |\sin(\pi q/Q)|. \qquad (30)$$

We have checked that this expression reproduces very accurately the lower branch of the spectrum in the regime where $m_e \to 1$ and $\eta \ll -\frac{1}{2}\ln(1 - m_e)$ (see Appendix C).

Finally, we examined the regions of the spectrum where two different bands approach each other and tried to determine whether they cross or not. Our numerical results suggest that there is no gap separating any couple of adjacent bands, and thus we are in the presence of the phenomenon of level crossing. Hence, the usual argument of gap opening because of Bragg scattering at the boundary of the Brillouin zone [59] does not seem to apply here, presumably because cnoidal waves do not scatter linear excitations.

C. Dynamic structure factor and sum rules

The dynamic structure factor provides important information on the dynamic behavior of the system. It is given by

$$S(q,\omega) = \sum_{\ell=1}^{\infty} |\langle 0|\delta\rho_q|\ell\rangle|^2 \delta(\hbar\omega - \hbar\omega_{\ell,q}), \qquad (31)$$

where the sum is extended over all the bands and $\delta\rho_q$ is the q component of the density fluctuation operator. Its matrix operator between the ground state $|0\rangle$ and the ℓth excited band $|\ell\rangle$ can be easily computed, $\langle 0|\delta\rho_q|\ell\rangle = \int_{-\Lambda/2}^{\Lambda/2} dx\, \delta\tilde{n}_{\ell,q}(x)e^{-iqx} = \Lambda\delta\tilde{n}_{\ell,q,0}$, where $\delta\tilde{n}_{\ell,q,0}$ is the $\nu = 0$ coefficient in the Bloch-wave expansion of Eq. (B3a).

---

[2]Similar negative-frequency modes, although of discrete nature, have been found in soliton trains trapped in ring geometries [34].
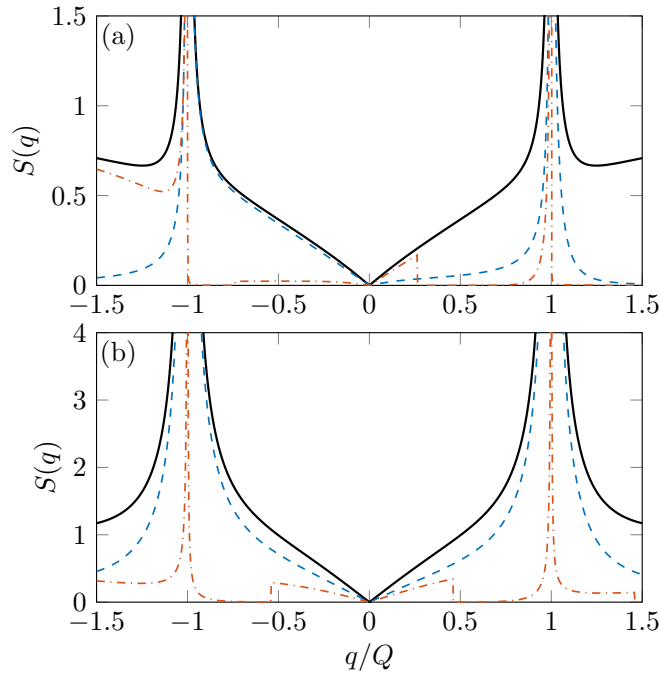
FIG. 5. Static structure factor as a function of q (black solid lines). The blue dashed and red dash-dotted curves show the contributions of the lower and upper gapless bands, respectively, for cases corresponding to the same values of m_e and η as in Fig. 4: (a) $\eta = 0.6$ and $m_e = 0.5$ and (b) $\eta = 2.0$ and $m_e = 0.8$.
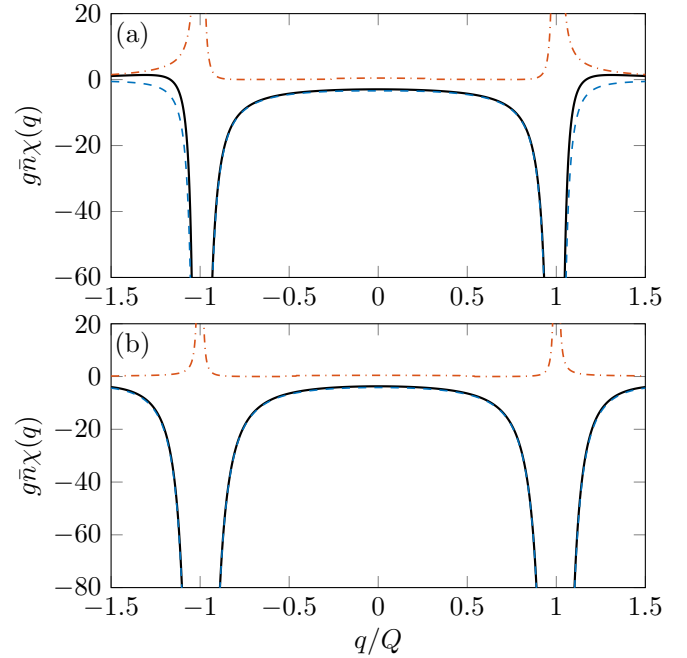

FIG. 6. Compressibility as a function of q (black solid lines). The blue dashed and red dash-dotted lines show the contributions of the lower and upper gapless bands, respectively, for cases corresponding to the same values of m_e and η as in Fig. 4: (a) $\eta = 0.6$ and $m_e = 0.5$ and (b) $\eta = 2.0$ and $m_e = 0.8$.

For a given integer p one defines the pth moment of the dynamic structure factor as [56]

$$
\begin{aligned}
m_p(q) &= \hbar^{p+1} \int_{-\infty}^{+\infty} d\omega\, \omega^p S(q, \omega) \\
&= \sum_{\ell=1}^{\infty} (\hbar\omega_{\ell,q})^p |\langle 0|\rho_q|\ell\rangle|^2.
\end{aligned}
\tag{32}
$$

We first consider the $p = 0$ moment $m_0(q) = N_\Lambda S(q)$, where we have introduced the static structure factor

$$
S(q) = N_\Lambda^{-1} \sum_{\ell=1}^{\infty} |\langle 0|\rho_q|\ell\rangle|^2.
\tag{33}
$$

We plot $S(q)$ in Fig. 5 for the same values of the parameters as Fig. 4. We also plot the contributions of the two gapless bands (sometimes referred to as the strengths of $\delta\rho_q$). These contributions are not symmetric under inversion of q into $-q$ for the same reason the spectra of Fig. 4 are not; however, as was shown in Ref. [66], the full static structure factor is symmetric as a consequence of its definition, regardless of the properties of the ground state.

The contributions of the gapless bands to $S(q)$ are dominant at small $|q|$. For a shallow cnoidal wave (small m_e) the lower gapless band ($\ell = 1$) exhausts $S(q)$ at $q < 0$ and the upper one ($\ell = 2$) at $q > 0$, as visible in Fig. 5(a). This behavior has the same explanation as that of the excitation spectrum (see Sec. IV B), namely, it stems from the closeness of these shallow waves to uniform gases. It is also shared by all the moments $m_p(q)$ with $p \neq 0$. As m_e increases, the strength of the lower band grows significantly and eventually,

at high m_e, it dominates $S(q)$ in a wide range of q (both positive and negative), as shown in Fig. 5(b).

Another remarkable feature is that the strengths of both gapless bands [and consequently $S(q)$ itself] diverge when q equals an integer multiple of Q, i.e., at the edges of each Brillouin zone (except at $q = 0$). An analogous behavior occurs for the supersolid phase of dipolar gases [67,68], as well as for the stripe phase of spin-orbit-coupled Bose-Einstein condensates [57], where, using sum-rule arguments, it was shown that the existence of a nonzero crystalline order parameter causes a $|q - Q|^{-1}$ divergence of $S(q)$ at the boundary of the first Brillouin zone.

The $p = -1$ moment is related to the compressibility $\chi(q)$ by

$$
m_{-1}(q) + m_{-1}(-q) = N_\Lambda \chi(q).
\tag{34}
$$

The behavior of the compressibility, as well as that of the contributions of the two gapless bands, is displayed in Fig. 6. Notice that $\chi(q)$ is dominated by the lowest negative-frequency band for a wide range of values about $q = 0$ and is thus itself negative in this range, revealing once more the presence of an energetic instability. Like the static structure factor, it diverges at the edges of the Brillouin zones except $q = 0$, again in agreement with the findings of Ref. [57]. Interestingly, as illustrated in Fig. 6, the negative divergence of the total $\chi(q)$ is caused by the contribution of the $\ell = 1$ band, whereas the $\ell = 2$ term is positively divergent. One can better understand this aspect using a sum-rule argument. From the inequality $\hbar\omega_{1,q} m_{-1}(q) \leqslant m_0(q)$, which holds even

for negative $\omega_{1,q}$, it follows that

$$\chi(q) \geqslant \left(\frac{1}{\hbar\omega_{1,q}} + \frac{1}{\hbar\omega_{1,-q}} \right) S(q). \qquad (35)$$

The right-hand side of Eq. (35) approximates well $\chi(q)$ when q is close to $\pm Q$ and the static structure factor is exhausted by the $\ell = 1$ term; it negatively diverges as $q \to \pm Q$ because the prefactor of $S(q)$ is negative. This divergence is however mitigated by the contributions of the positive-frequency modes, which is again consistent with the inequality (35).

Finally, we have checked that the $p = 1$ moment satisfies the f-sum rule $m_1(q) + m_1(-q) = N_\Lambda \hbar^2 q^2/m$ [56]. Different from the sum rules discussed previously, for large m_e and small $|q|$ the f-sum rule is dominated mainly by the upper gapless band. This is because the lower band, despite having bigger strength, has much smaller frequency (in absolute value) than the upper one in this regime.

V. CONCLUSION

We have studied several relevant features of an ultracold Bose gas in a cnoidal-wave state. The equilibrium wave function is characterized by periodic spatial density modulations described in terms of Jacobi's elliptic functions. Cnoidal waves spontaneously break both U(1) and continuous translational symmetry, thus exhibiting typical supersolid features. In addition, as argued by Leggett [11,45], their superfluid fraction is depleted even at zero temperature and gets smaller and smaller as the contrast of the fringes increases. A further signature of supersolidity is represented by the behavior of the excitation spectrum, featuring a band structure with two gapless bands. The latter exhibit a mixed phase and crystal character. The presence of a crystalline structure causes the divergence of the static structure factor and the compressibility at the edges of the Brillouin zones.

The configurations studied in the present work are reminiscent of the Abrikosov lattice in a two-dimensional system. However, in the latter case one has a redundancy among the Nambu-Goldstone bosons [69], leading to a spectrum with a single quadratic mode. Interestingly, the same does not occur in our case and indeed two (linear) modes are present in the spectrum, related to the U(1) and translational symmetries.

Our results open alternative perspectives for the study of supersolidity in ultracold atomic gases. Cnoidal waves are excited states that could be realized, for instance, moving an obstacle into the gas at an appropriate speed [70–75]. The density modulations can be probed either *in situ* or after time of flight. The excitation spectrum and the dynamic structure factor can then be accessed using two-photon Bragg spectroscopy.

The spectrum of a cnoidal wave demonstrates dynamic stability (all the eigenvalues are real) and, more importantly, energetic instability (some of the eigenvalues are negative). This aspect may be relevant in the context of analog gravity: It has been shown [39,75] that in some circumstances, an obstacle moving at supersonic speed in a Bose-Einstein condensate may give rise to an upstream cnoidal wave and a downstream supersonic flat density pattern, both stationary in the reference frame of the obstacle. It would then be of great interest to study the analogous Hawking radiation in this realistic and experimentally relevant setting, where negative-norm modes exist on both sides of the acoustic pseudohorizon [76].

We finally note that various types of cnoidal waves have already been experimentally realized in the framework of nonlinear optics, for both repulsive and attractive interactions, in the out-of-equilibrium context of nonlinear whispering-gallery mode resonators [77–80], but also in two-dimensional photorefractive media [81,82] and in optical fibers [83]. We believe it should be possible to study supersolidity phenomena in such settings, even in the presence of dissipation, as has been done for superfluidity in nonequilibrium systems of condensed microcavity polaritons [84].

ACKNOWLEDGMENTS

APPENDIX A: LIMITING CASES

As discussed in Ref. [30], the cnoidal-wave solution admits several important limiting cases. In this Appendix we focus on the uniform and linear-wave limit at small m_e, as well as on the dark-soliton limit corresponding to $m_e \to 1$.

1. Uniform limit

Let us first look at the $m_e = 0$ case. In this situation the amplitude of the density oscillations vanishes. In addition, the velocity (22) simplifies to $\bar{v} = \pm c\sqrt{1 + \eta}$. This yields $\eta = \eta_0$ with $\eta_0 = \bar{v}^2/c^2 - 1$ and implies that the flow is supersonic, i.e., $|\bar{v}| \geqslant c$ (recall that $\eta > 0$ by definition). The chemical potential (10a) takes the standard form $\mu = g\bar{n} + m\bar{v}^2/2$ (the same happens in the linear-wave and dark-soliton limits discussed below).

2. Linear-wave limit

At first order in m_e one can approximate $\Gamma(m_e) - 1 \simeq -m_e/2$ and replace the sn function with an ordinary sine in Eq. (20). As a consequence, in this limit (nonlinear) cnoidal waves reduce to (linear) sinusoidal waves,

$$\frac{n(x)}{\bar{n}} \simeq 1 - \frac{\eta_0 m_e}{2} \cos(Q_0 x), \qquad (A1)$$

$$\Theta(x) \simeq \frac{m\bar{v}x}{\hbar} \pm \frac{\sqrt{\eta_0(1 + \eta_0)}m_e}{4} \sin(Q_0 x), \qquad (A2)$$

where $Q_0 = 2\sqrt{\eta_0}/\xi = 2m\sqrt{\bar{v}^2 - c^2}/\hbar$.

It is interesting to study these waves in a frame where they travel with a given phase velocity V. In such a frame, at every point in space the density and the velocity field oscillate in time with frequency $\Omega_0 = Q_0 V$. Let us set $\bar{v} = \bar{v}' - V$, where $\bar{v}'$ is the average velocity in the new frame. One can invert the definition of Q_0 given just above to express V, and hence Ω_0,

as a function of $\bar{v}'$ and Q_0. One finds the two values

$$\hbar\Omega_0(Q_0) = \hbar Q_0\bar{v}' \mp \sqrt{\frac{\hbar^2 Q_0^2}{2m}\left(\frac{\hbar^2 Q_0^2}{2m} + 2g\bar{n}\right)}. \quad (A3)$$

These are the two branches of the Bogoliubov spectrum of the uniform condensate discussed in the preceding section (which flows with velocity $\bar{v}'$ in the new frame). In addition, the ratio between the amplitudes of the phase and density modulations is $\mp\sqrt{(1+\eta_0)/4\eta_0} = \mp m|\Omega_0 - Q_0\bar{v}'|/\hbar Q_0^2$, in agreement with the prediction of the Bogoliubov theory [56]. We thus conclude that in the small-m_e limit traveling cnoidal waves describe standard Bogoliubov modes.

3. Dark-soliton limit

In the $m_e \to 1$ limit one has $\Gamma(m_e) \to 0$ and the sn function approaches the hyperbolic tangent. The velocity (22) becomes $\bar{v} = \pm c\sqrt{1-\eta}$. This gives $\eta = 1 - \bar{v}^2/c^2$, together with the condition of subsonic flow $|\bar{v}| \leqslant c$. Thus, the density and phase turn into those of a dark soliton [55,56], written in the frame where the latter is at rest and the background has velocity $\bar{v}$:

$$\frac{n(x)}{\bar{n}} = 1 - \frac{\cos^2\theta}{\cosh^2[\cos(\theta)x/\xi]}, \quad (A4)$$

$$\Theta(x) = \frac{m\bar{v}x}{\hbar} + \arctan\left[\frac{\tanh[\cos(\theta)x/\xi]}{\tan\theta}\right]. \quad (A5)$$

Here we have set $\sin\theta = \bar{v}/c$ and $\cos\theta = \sqrt{\eta}$, with $\theta \in [-\pi/2, \pi/2]$. In particular, when $\bar{v} = 0$ one obtains a black soliton, whose density vanishes at the center.

APPENDIX B: CALCULATION OF THE BOGOLIUBOV FREQUENCIES AND AMPLITUDES

In this Appendix we present the method we have used for solving the Bogoliubov equations (27). Using the ansatz (28) and equating the coefficients of $e^{-i\omega t}$ and $e^{i\omega t}$ on both sides, they can be cast in matrix form as follows:

$$\begin{pmatrix} \mathcal{B}^{(nn)} & \mathcal{B}^{(n\Theta)} \\ \mathcal{B}^{(\Theta n)} & \mathcal{B}^{(\Theta\Theta)} \end{pmatrix}\begin{pmatrix} \delta\tilde{n} \\ \delta\tilde{\Theta} \end{pmatrix} = \omega\begin{pmatrix} \delta\tilde{n} \\ \delta\tilde{\Theta} \end{pmatrix}. \quad (B1)$$

Here we have defined the four operators

$$\mathcal{B}^{(nn)} = -\frac{i\hbar}{m}\left(\Theta_x\frac{d}{dx} + \Theta_{xx}\right), \quad (B2a)$$

$$\mathcal{B}^{(n\Theta)} = -\frac{i\hbar}{m}\left(n\frac{d^2}{dx^2} + n_x\frac{d}{dx}\right), \quad (B2b)$$

$$\mathcal{B}^{(\Theta n)} = \frac{i\hbar}{4m}\left(n^{-1}\frac{d^2}{dx^2} - \frac{n_x}{n^2}\frac{d}{dx} + \frac{n_x^2 - nn_{xx}}{n^3}\right) - \frac{ig}{\hbar}, \quad (B2c)$$

$$\mathcal{B}^{(\Theta\Theta)} = -\frac{i\hbar\Theta_x}{m}\frac{d}{dx}. \quad (B2d)$$

Because of the periodicity of the coefficients entering these operators, the solutions of Eq. (B1) can be expressed as Bloch waves,

$$\delta\tilde{n}_{\ell,q}(x) = e^{iqx}\sum_{\nu\in\mathbb{Z}}\delta\tilde{n}_{\ell,q,\nu}e^{i\nu Qx}, \quad (B3a)$$

$$\delta\tilde{\Theta}_{\ell,q}(x) = e^{iqx}\sum_{\nu\in\mathbb{Z}}\delta\tilde{\Theta}_{\ell,q,\nu}e^{i\nu Qx}. \quad (B3b)$$

Here q denotes the quasimomentum, $\delta\tilde{n}_{\ell,q,\nu}$ and $\delta\tilde{\Theta}_{\ell,q,\nu}$ are Fourier expansion coefficients, and the sums run over all integer ν. As explained in Sec. IV B, the band index ℓ is needed to distinguish between different solutions at fixed q.

We now derive a set of equations that allow one to calculate the expansion coefficients $\delta\tilde{n}_{\ell,q,\nu}$ and $\delta\tilde{\Theta}_{\ell,q,\nu}$ for each Bogoliubov mode, as well as the corresponding frequency $\omega_{\ell,q}$. For this purpose, we need the Fourier expansions of the coefficients of operators (B2). This analysis can be simplified by recalling that $-n_x/n^2 = (n^{-1})_x$, $\Theta_x = m\mathcal{J}\hbar^{-1}n^{-1}$, $\Theta_{xx} = m\mathcal{J}\hbar^{-1}(n^{-1})_x$, and

$$\frac{n_x^2 - nn_{xx}}{n^3} = \frac{1}{2}\left[(n^{-1})_{xx} - \frac{n_{xx}}{n^2}\right]$$
$$= \frac{(n^{-1})_{xx}}{2} - \frac{3mg}{\hbar^2} + \frac{4m\mu}{\hbar^2 n} - \frac{2m\mathcal{E}}{\hbar^2 n^2}.$$

The expressions of μ, $\mathcal{E}$, and $\mathcal{J}$ are provided in Eqs. (10). Thus, we only need to determine the expansion of the density $n(x) = \sum_{\nu\in\mathbb{Z}}\tilde{n}_\nu^{(1)}e^{i\nu Qx}$, of its inverse $n^{-1}(x) = \sum_{\nu\in\mathbb{Z}}\tilde{n}_\nu^{(-1)}e^{i\nu Qx}$, and of the squared inverse $n^{-2}(x) = \sum_{\nu\in\mathbb{Z}}\tilde{n}_\nu^{(-2)}e^{i\nu Qx}$. Fourier coefficients of powers and rational fractions of Jacobi's elliptic functions have been widely studied in the literature [85,86]. For $\nu = 0$ one finds

$$\tilde{n}_0^{(1)} = \bar{n}, \quad (B4a)$$

$$\tilde{n}_0^{(-1)} = (f_s\bar{n})^{-1}, \quad (B4b)$$

$$\tilde{n}_0^{(-2)} = \frac{(n_3 - n_1)\Gamma(m_e) - n_3}{2n_1 n_2 n_3}$$
$$+ \frac{n_1 n_2 + n_2 n_3 + n_3 n_1}{2n_1 n_2 n_3}(f_s\bar{n})^{-1}, \quad (B4c)$$

where f_s is the superfluid fraction defined in Eq. (23). Instead, the $\nu \neq 0$ coefficients read

$$\tilde{n}_\nu^{(1)} = -\frac{\pi^2(n_3 - n_1)}{2K^2(m_e)}\frac{\nu}{\sinh(\nu w)}, \quad (B5a)$$

$$\tilde{n}_\nu^{(-1)} = \frac{\pi}{2K(m_e)}\sqrt{\frac{n_3 - n_1}{n_1 n_2 n_3}}\frac{\sinh(\nu w_0)}{\sinh(\nu w)}, \quad (B5b)$$

$$\tilde{n}_\nu^{(-2)} = \frac{(n_1 n_2 + n_2 n_3 + n_3 n_1)\tilde{n}_\nu^{(-1)} - \cosh(\nu w_0)\tilde{n}_\nu^{(1)}}{2n_1 n_2 n_3}. \quad (B5c)$$

Here we have defined $w = \pi K(1 - m_e)/K(m_e)$ and $w_0 = \pi[K(1 - m_e) - K_0]/K(m_e)$, where $0 < K_0 < K(1 - m_e)$ is the solution of the equation $\mathrm{cn}(K_0, 1 - m_e) = \sqrt{(n_2 - n_1)/n_2}$.

We now insert the Bloch-wave ansatz (B3) into the coupled equations (B1) and use the above results to expand the coefficients of the operators (B2) in Fourier series. Then we equate the terms on the two sides of the resulting equations that oscillate in space with the same wave vector. This yields an infinite set of coupled algebraic equations involving the

expansion coefficients $\delta\tilde{n}_{\ell,q,\nu}$ and $\delta\tilde{\Theta}_{\ell,q,\nu}$, as well as the corresponding excitation frequencies $\omega_{\ell,q}$. This set can be written in a compact form by defining the two infinite-dimensional column vectors

$$\delta\tilde{\mathfrak{n}}_{\ell,q} = (\cdots \delta\tilde{n}_{\ell,q,\nu-1}\delta\tilde{n}_{\ell,q,\nu}\delta\tilde{n}_{\ell,q,\nu+1}\cdots)^T,$$

$$\delta\tilde{\Theta}_{\ell,q} = (\cdots \delta\tilde{\Theta}_{\ell,q,\nu-1}\delta\tilde{\Theta}_{\ell,q,\nu}\delta\tilde{\Theta}_{\ell,q,\nu+1}\cdots)^T.$$

The normalization condition for $\delta\tilde{\mathfrak{n}}_{\ell,q}$ and $\delta\tilde{\Theta}_{\ell,q}$ follows from Eq. (29) and reads $i\Lambda(\delta\tilde{\mathfrak{n}}_{\ell,q}^\dagger\delta\tilde{\Theta}_{\ell,q} - \delta\tilde{\Theta}_{\ell,q}^\dagger\delta\tilde{\mathfrak{n}}_{\ell,q}) = 1$. The above procedure leads to the eigenvalue equation

$$\begin{pmatrix} \mathsf{B}^{(nn)}(q) & \mathsf{B}^{(n\Theta)}(q) \\ \mathsf{B}^{(\Theta n)}(q) & \mathsf{B}^{(\Theta\Theta)}(q) \end{pmatrix}\begin{pmatrix} \delta\tilde{\mathfrak{n}}_{\ell,q} \\ \delta\tilde{\Theta}_{\ell,q} \end{pmatrix} = \omega_{\ell,q}\begin{pmatrix} \delta\tilde{\mathfrak{n}}_{\ell,q} \\ \delta\tilde{\Theta}_{\ell,q} \end{pmatrix}, \quad \text{(B6)}$$

where the B's are infinite-dimensional matrices with entries

$$\mathsf{B}_{\nu_1\nu_2}^{(nn)}(q) = \mathcal{J}\tilde{n}_{\nu_1-\nu_2}^{(-1)}(q + \nu_1 Q), \quad \text{(B7a)}$$

$$\mathsf{B}_{\nu_1\nu_2}^{(n\Theta)}(q) = \frac{i\hbar}{m}\tilde{n}_{\nu_1-\nu_2}^{(1)}(q + \nu_1 Q)(q + \nu_2 Q), \quad \text{(B7b)}$$

$$\mathsf{B}_{\nu_1\nu_2}^{(\Theta n)}(q) = -\frac{i\hbar}{4m}\tilde{n}_{\nu_1-\nu_2}^{(-1)}$$
$$\times\left[q^2 + (\nu_1 + \nu_2)Qq + \frac{(\nu_1^2 + \nu_2^2)Q^2}{2} \right]$$
$$- \frac{7ig}{4\hbar}\delta_{\nu_1,\nu_2} + \frac{i\mu}{\hbar}\tilde{n}_{\nu_1-\nu_2}^{(-1)} - \frac{i\mathcal{E}}{2\hbar}\tilde{n}_{\nu_1-\nu_2}^{(-2)}, \quad \text{(B7c)}$$

$$\mathsf{B}_{\nu_1\nu_2}^{(\Theta\Theta)}(q) = \mathcal{J}\tilde{n}_{\nu_1-\nu_2}^{(-1)}(q + \nu_2 Q). \quad \text{(B7d)}$$

Numerically solving Eq. (B6), one recovers all the results of Sec. IV. Of course, in order to reduce the problem to a finite-dimensional one it is necessary to fix a cutoff $\nu_{\max}$ and truncate all the above Fourier expansions retaining only the terms with $-\nu_{\max} \leqslant \nu \leqslant \nu_{\max}$. The choice of the best value of $\nu_{\max}$ depends on m_e and η. At fixed η and small m_e, where cnoidal waves do not significantly deviate from linear waves, taking $\nu_{\max}$ equal to 5 or 6 can be sufficient to achieve good accuracy in the results. Conversely, increasing m_e one needs larger and larger values of $\nu_{\max}$. These can even exceed 100 when the cnoidal wave is close to the soliton limit (for $\eta \leqslant 1$) or its contrast is close to 1 (for $\eta > 1$).

APPENDIX C: LOWER EXCITATION BRANCH OF A TRAIN OF DARK SOLITONS

In the regime where the period Λ of the cnoidal wave is large compared to the width $\xi/\sqrt{\eta}$ of a dark soliton, the cnoidal wave can be considered as a train of regularly spaced identical solitons. From Eq. (16) this occurs when $K(m_e) \gg 1$, i.e., when m_e is close to unity. Since solitons are essentially classical objects, it is natural to expect that, in this regime, the lowest branch of the spectrum should be described as an excitation of an array of classical particles connected by springs. Denoting by Ω the resonant angular frequency associated with these springs, the corresponding spectrum is of the form [59]

$$\omega_{1,q} = -2\Omega|\sin(q\Lambda/2)|. \quad \text{(C1)}$$

The value of Ω depends on the interaction between two solitons and on their inertial mass. It can be determined by means of Manton's method [87,88] as explained now.

For studying the interaction between two solitons, one considers a configuration where the solitons are stationary, in a background with subsonic velocity $\bar{v}$ and otherwise uniform density $\bar{n}$. It is convenient to single out the velocity of the background and to write $\psi(x,t) = \phi(x,t)\exp(ikx)$, where $k = m\bar{v}/\hbar$. Then one has in (1) $\mu = \hbar^2 k^2/2m + g\bar{n}$ and ϕ is the solution of

$$i\hbar\phi_t = -\frac{\hbar^2}{2m}\phi_{xx} - i\frac{\hbar^2 k}{m}\phi_x + g(|\phi|^2 - \bar{n})\phi. \quad \text{(C2)}$$

An ansatz describing two identical stationary solitons separated by a distance Δ is of the form

$$\phi(x) = \sqrt{\bar{n}}\Phi(x)\Phi(x - \Delta), \quad \text{(C3)}$$

where

$$\Phi(x) = \cos\theta\tanh[\cos(\theta)x/\xi] - i\sin\theta, \quad \text{(C4)}$$

with $\theta \in [-\pi/2, \pi/2]$. Recall that $\sqrt{\bar{n}}\Phi(x)$ describes a stationary isolated soliton, the solution of Eq. (C2). The soliton is stationary because its velocity $V = -c\sin\theta$ is exactly opposed to the velocity $\bar{v} = c\sin\theta$ of the background. Note that, up to a global phase factor, one has $\sqrt{\bar{n}}\Phi(x)\exp(ikx) = \sqrt{\bar{n}}e^{i\Theta}$, with $n(x)$ and $\Theta(x)$ given by Eqs. (A4) and (A5), respectively. As regards the two-soliton case, of course the ansatz (C3) is not an exact solution of the Gross-Pitaevskii equation (C2), but it is expected to be a reasonable approximation if[3] $\Delta\cos\theta \gg \xi$.

The Lagrangian density associated with the Gross-Pitaevskii equation (C2) is

$$\mathcal{L} = \frac{i\hbar}{2}(\phi^*\phi_t - \phi_t^*\phi)(1 - \bar{n}|\phi|^{-2}) - \frac{\hbar^2}{2m}|\phi_x|^2$$
$$- \frac{i\hbar^2 k}{2m}(\phi_x^*\phi - \phi^*\phi_x) - \frac{g}{2}(|\phi|^2 - \bar{n})^2. \quad \text{(C5)}$$

Note the unfamiliar multiplicative term $(1 - \bar{n}|\phi|^{-2})$ in the first term of the above expression. It corresponds to adding to the usual Lagrangian density a total derivative which does not affect the form of the Gross-Pitaevskii equation (C2) but yields the correct physical momentum of a soliton [56,89–92], namely,

$$P = \hbar\bar{n}(\pi + 2\theta + \sin 2\theta), \quad \text{(C6)}$$

for a soliton of type (C4).

Considering two points a and b located around the soliton centered at Δ ($a < \Delta < b$), one has

$$\frac{d}{dt}\int_a^b dx\,\mathcal{P}(x,t) = \mathcal{T}(a,t) - \mathcal{T}(b,t), \quad \text{(C7)}$$

where $\mathcal{P} = \frac{i\hbar}{2}(\phi\phi_x^* - \phi^*\phi_x)(1 - \bar{n}|\phi|^{-2})$ is the momentum density and

$$\mathcal{T} = \frac{i\hbar}{2}(\phi^*\phi_t - \phi\phi_t^*)(1 - \bar{n}|\phi|^{-2})$$
$$+ \frac{\hbar^2}{2m}|\phi_x|^2 - \frac{g}{2}(|\phi|^2 - \bar{n})^2 \quad \text{(C8)}$$

---

[3]We will argue at the end of this Appendix that the regime of validity of the ansatz (C3) needs to be defined more carefully.
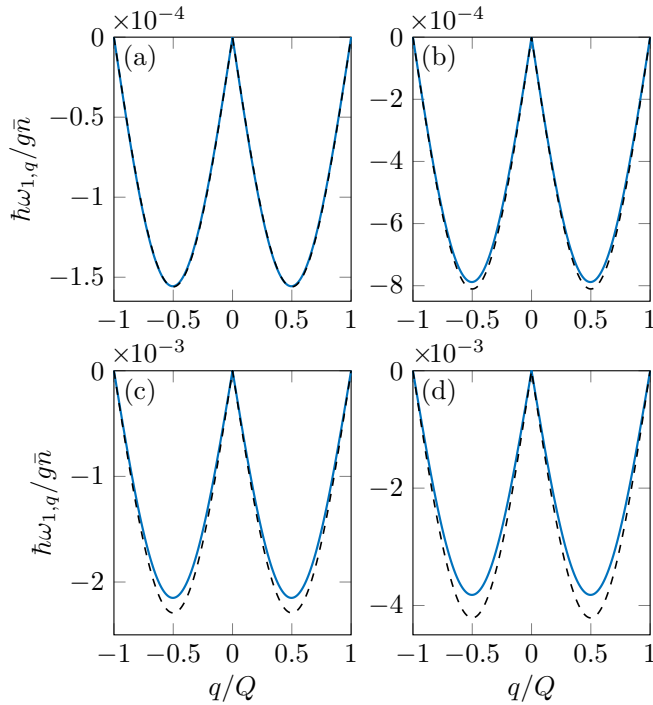
FIG. 7. Lowest band of the excitation spectrum as a function of q. In each panel we compare the numerical results (blue solid curve) with the analytic prediction (30) (black dashed curve) at $m_e = 0.99$, i.e., close to the dark-soliton limit. We take η equal to (a) 0.1, (b) 0.3, (c) 0.6, and (d) 0.9.

FIG. 8. Density profiles of the cnoidal wave for $m_e = 0.99$ and different values of η, corresponding to the same values of η as in Fig. 7: (a) 0.1, (b) 0.3, (c) 0.6, and (d) 0.9.

the stress tensor, both associated with the Lagrangian density (C5). If $\Delta - a$ and $b - \Delta$ are large compared to $\xi / \cos \theta$, then the left-hand side of Eq. (C7) can be identified with the time derivative $dP/dt = 4\hbar \bar{n} \dot{\theta} \cos^2 \theta$ of the momentum (C6) of the soliton centered around Δ. Manton's method amounts to identifying, on the right-hand side of Eq. (C7), the contribution due to the soliton centered at the origin, from which one can infer the force exerted by one soliton onto the other. Retaining only the leading order of this contribution and discarding all the other contributions leads to

$$\hbar \dot{\theta} \simeq -8g\bar{n} \cos^4 \theta \exp(-2\Delta \cos \theta / \xi). \quad \text{(C9)}$$

In this formula $\dot{\theta}$ can be expressed in terms of the time derivative of the velocity $V = -c \sin \theta$ of the soliton with respect to the background. The fact that V changes means that the soliton under scrutiny does not remain stationary and moves with an acceleration $\ddot{\Delta} = \dot{V} = -c\dot{\theta} \cos \theta = f(\Delta)$, where f, which is easily evaluated from Eq. (C9), is the ratio of the force experienced by the soliton centered around Δ to its inertial mass $m_I = -4m\xi\bar{n} \cos \theta$ (see Ref. [93]). Both the force and the mass are negative and this results in a repulsive interaction between the solitons.

Once the interaction between two dark solitons has been determined, it is easy to turn to the case of a chain of solitons, considered as a one-dimensional lattice of classical particles. For determining the elementary excitations of such a system, one writes the spacing between two successive solitons as $\Delta(t) = \Lambda + X(t)$ and the angular frequency Ω of the equiva-
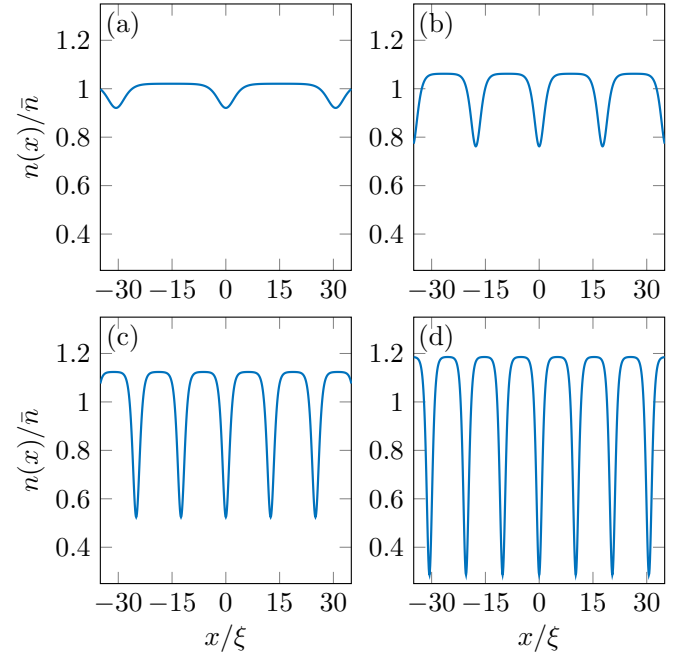
lent spring is just

$$\Omega = \sqrt{\left. -\frac{df}{d\Delta} \right|_{X=0}} = \frac{4c}{\xi} \cos^3 \theta \exp(-\Lambda \cos \theta / \xi), \quad \text{(C10)}$$

which, together with Eq. (C1), yields the result (30) in the regime where the cnoidal wave becomes a chain of well-separated solitons. In this regime, the spacing between nearest solitons being large, the intensity of their interaction is weak and the lowest branch has a decreasing amplitude; in the dark-soliton limit of Sec. V it becomes a zero mode corresponding to the translational degree of freedom of an isolated soliton.

The accuracy of the approximation (30) is illustrated in Fig. 7 in the case of a cnoidal wave with $m_e = 0.99$ for several values of η, ranging from 0.1 to 0.9. As one can see, the agreement is excellent for low values of η and becomes less accurate when η increases. This could be considered strange because we repeatedly stated that the validity of our approximation should only rely on the fact that the separation Λ between two successive solitons is large compared to the soliton's width $\xi / \cos \theta$ and the ratio of these two quantities only depends on m_e, not on η [see Eq. (16)].

This conundrum is solved by inspecting the two-soliton ansatz (C3). This ansatz is valid for evaluating the interaction between two nearest solitons inasmuch as the ground state of the train of solitons itself can be described by an approximate wave function of the type

$$\phi(x) = \sqrt{\bar{n}} \prod_{j \in \mathbb{Z}} \Phi(x - j\Lambda). \quad \text{(C11)}$$

From the density profiles plotted in Fig. 8, it is clear that the validity of expression (C11) decreases for increasing values of η, since the density n_2 of the flat region between two

solitons significantly exceeds $\bar{n}$ as η increases, contrarily to the situation depicted by Eq. (C11). From the expression (19b) one sees that, in the regime $0 < 1 - m_e \ll 1$, n_2 remains close to $\bar{n}$ when the additional condition

$$\eta \ll -\tfrac{1}{2}\ln(1 - m_e) \qquad (C12)$$

is fulfilled. For the value $m_e = 0.99$ corresponding to the plots of Figs. 7 and 8, the right-hand side of this inequality is equal to 2.3. This is the reason why the approximation (30) starts being less accurate when $\eta = 0.6$ [see Fig. 7(c)].

[1] S. Balibar, The enigma of supersolidity, Nature (London) **464**, 176 (2010).

[2] M. Boninsegni and N. V. Prokof'ev, *Colloquium:* Supersolids: What and where are they? Rev. Mod. Phys. **84**, 759 (2012).

[3] V. I. Yukalov, Saga of superfluid solids, Physics **2**, 49 (2020).

[4] F. Böttcher, J.-N. Schmidt, J. Hertkorn, K. S. H. Ng, S. D. Graham, M. Guo, T. Langen, and T. Pfau, New states of matter with fine-tuned interactions: Quantum droplets and dipolar supersolids, Rep. Prog. Phys. **84**, 012403 (2020).

[5] O. Penrose and L. Onsager, Bose-Einstein condensation and liquid helium, Phys. Rev. **104**, 576 (1956).

[6] E. P. Gross, Unified theory of interacting bosons, Phys Rev. **106**, 161 (1957).

[7] E. P. Gross, Classical theory of boson wave fields, Ann. Phys. (NY) **4**, 57 (1958).

[8] D. J. Thouless, The flow of a dense superfluid, Ann. Phys. (NY) **52**, 403 (1969).

[9] A. F. Andreev and I. M. Lifshitz, Quantum theory of defects in crystals, Zh. Eksp. Teor. Fiz. **56**, 2057 (1969) [Sov. Phys. JETP **29**, 1107 (1969)].

[10] G. V. Chester, Speculations on Bose-Einstein condensation and quantum crystals, Phys. Rev. A **2**, 256 (1970).

[11] A. J. Leggett, Can a Solid Be "Superfluid"? Phys. Rev. Lett. **25**, 1543 (1970).

[12] D. A. Kirzhnits and Y. A. Nepomnyashchii, Coherent crystallization of quantum liquid, Zh. Eksp. Teor. Fiz. **59**, 2203 (1971) [Sov. Phys. JETP **32**, 1191 (1971)].

[13] L. P. Pitaevskii, Layered structure of superfluid ^{4}He with supercritical motion, Pis'ma Zh. Eksp. Teor. Fiz. **39**, 423 (1984) [JETP Lett. **39**, 511 (1984)].

[14] Y. Pomeau and S. Rica, Dynamics of a Model of Supersolid, Phys. Rev. Lett. **72**, 2426 (1994).

[15] J. Nyéki, A. Phillis, A. Ho, D. Lee, P. Coleman, J. Parpia, B. Cowan, and J. Saunders, Intertwined superfluid and density wave order in two-dimensional ^{4}He, Nat. Phys. **13**, 455 (2017).

[16] J. Léonard, A. Morales, P. Zupancic, T. Esslinger, and T. Donner, Supersolid formation in a quantum gas breaking continuous translational symmetry, Nature (London) **543**, 87 (2017).

[17] J. Li, J. Lee, W. Huang, S. Burchesky, B. Shteynas, F. Ç. Top, A. O. Jamison, and W. Ketterle, A stripe phase with supersolid properties in spin-orbit-coupled Bose-Einstein condensates, Nature (London) **543**, 91 (2017).

[18] L. Tanzi, E. Lucioni, F. Famà, J. Catani, A. Fioretti, C. Gabbanini, R. N. Bisset, L. Santos, and G. Modugno, Observation of a Dipolar Quantum Gas with Metastable Supersolid Properties, Phys. Rev. Lett. **122**, 130405 (2019).

[19] F. Böttcher, J.-N. Schmidt, M. Wenzel, J. Hertkorn, M. Guo, T. Langen, and T. Pfau, Transient Supersolid Properties in an Array of Dipolar Quantum Droplets, Phys. Rev. X **9**, 011051 (2019).

[20] L. Chomaz, D. Petter, P. Ilzhöfer, G. Natale, A. Trautmann, C. Politi, G. Durastante, R. M. W. van Bijnen, A. Patscheider, M. Sohmen, M. J. Mark, and F. Ferlaino, Long-Lived and Transient Supersolid Behaviors in Dipolar Quantum Gases, Phys. Rev. X **9**, 021012 (2019).

[21] G. Natale, R. M. W. van Bijnen, A. Patscheider, D. Petter, M. J. Mark, L. Chomaz, and F. Ferlaino, Excitation Spectrum of a Trapped Dipolar Supersolid and Its Experimental Evidence, Phys. Rev. Lett. **123**, 050402 (2019).

[22] L. Tanzi, S. M. Roccuzzo, E. Lucioni, F. Famá, A. Fioretti, C. Gabbanini, G. Modugno, A. Recati, and S. Stringari, Supersolid symmetry breaking from compressional oscillations in a dipolar quantum gas, Nature (London) **574**, 382 (2019).

[23] M. Guo, F. Böttcher, J. Hertkorn, J.-N. Schmidt, M. Wenzel, H. P. Büchler, T. Langen, and T. Pfau, The low-energy Goldstone mode in a trapped dipolar supersolid, Nature (London) **574**, 386 (2019).

[24] D. Petter, A. Patscheider, G. Natale, M. J. Mark, M. A. Baranov, R. V. Bijnen, S. M. Roccuzzo, A. Recati, B. Blakie, D. Baillie, L. Chomaz, and F. Ferlaino, High-energy Bragg scattering measurements of a dipolar supersolid, arXiv:2005.02213.

[25] L. Tanzi, J. G. Maloberti, G. Biagioni, A. Fioretti, C. Gabbanini, and G. Modugno, Evidence of superfluidity in a dipolar supersolid from non-classical rotational inertia, arXiv:1912.01910.

[26] P. Ilzhöfer, M. Sohmen, G. Durastante, C. Politi, A. Trautmann, G. Morpurgo, T. Giamarchi, L. Chomaz, M. J. Mark, and F. Ferlaino, Phase coherence in out-of-equilibrium supersolid states of ultracold dipolar atoms, arXiv:1912.10892.

[27] S. V. Iordanskii and L. P. Pitaevskii, Bose condensation of moving rotons, Usp. Fiz. Nauk **131**, 293 (1980) [Sov. Phys. Usp. **23**, 317 (1980)].

[28] F. Ancilotto, F. Dalfovo, L. P. Pitaevskii, and F. Toigo, Density pattern in supercritical flow of liquid ^{4}He, Phys. Rev. B **71**, 104530 (2005).

[29] G. Baym and C. J. Pethick, Landau critical velocity in weakly interacting Bose gases, Phys. Rev. A **86**, 023602 (2012).

[30] T. Tsuzuki, Nonlinear waves in the Pitaevskii-Gross equation, J. Low Temp. Phys. **4**, 441 (1971).

[31] D. J. Korteweg and G. de Vries, On the change of form of long waves advancing in a rectangular canal, and on a new type of long stationary waves, Philos. Mag. **39**, 422 (1895).

[32] M. Abramowitz and I. A. Stegun, *Handbook of Mathematical Functions with Formulas, Graphs, and Mathematical Tables* (Dover, New York, 1965).

[33] R. Kanamoto, L. D. Carr, and M. Ueda, Topological Winding and Unwinding in Metastable Bose-Einstein Condensates, Phys. Rev. Lett. **100**, 060401 (2008).

[34] R. Kanamoto, L. D. Carr, and M. Ueda, Metastable quantum phase transitions in a periodic one-dimensional Bose gas: Mean-field and Bogoliubov analyses, Phys. Rev. A **79**, 063616 (2009).

[35] M. K. Parit, G. Tyagi, D. Singh, and P. K. Panigrahi, Supersolid behavior in one-dimensional self-trapped Bose-Einstein condensate, arXiv:2004.09973.

[36] C. Menotti and S. Stringari, Collective oscillations of a one-dimensional trapped Bose-Einstein gas, Phys. Rev. A **66**, 043610 (2002).

[37] M. Olshanii, Atomic Scattering in the Presence of an External Confinement and a Gas of Impenetrable Bosons, Phys. Rev. Lett. **81**, 938 (1998).

[38] J. S. Langer and V. Ambegaokar, Intrinsic resistive transition in narrow superconducting channels, Phys. Rev. **164**, 498 (1967).

[39] P. Leboeuf and N. Pavloff, Bose-Einstein beams: Coherent propagation through a guide, Phys. Rev. A **64**, 033602 (2001).

[40] Y. G. Mamaladze and O. D. Cheshvili, Flow of a Superfluid Liquid in Porous Media, Zh. Eksp. Teor. Fiz. **50**, 169 (1966) [Sov. Phys. JETP **23**, 112 (1966)].

[41] P. Leboeuf, N. Pavloff, and S. Sinha, Solitonic transmission of Bose-Einstein matter waves, Phys. Rev. A **68**, 063608 (2003).

[42] P. G. de Gennes, *Superconductivity of Metals and Alloys* (CRC, Boca Raton, 2019).

[43] L. D. Carr, C. W. Clark, and W. P. Reinhardt, Stationary solutions of the one-dimensional nonlinear Schrödinger equation. I. Case of repulsive nonlinearity, Phys. Rev. A **62**, 063610 (2000).

[44] B. V. Svistunov, E. S. Babaev, and N. V. Prokof'ev, *Superfluid States of Matter* (CRC, Boca Raton, 2015).

[45] A. J. Leggett, On the superfluid fraction of an arbitrary many-body system at $T = 0$, J. Stat. Phys. **93**, 927 (1998).

[46] L. Chomaz, Probing the supersolid order via high-energy scattering: Analytical relations among the response, density modulation, and superfluid fraction, Phys. Rev. A **102**, 023333 (2020).

[47] S. M. Roccuzzo and F. Ancilotto, Supersolid behavior of a dipolar Bose-Einstein condensate confined in a tube, Phys. Rev A **99**, 041601(R) (2019).

[48] Y.-C. Zhang, F. Maucher, and T. Pohl, Supersolidity around a Critical Point in Dipolar Bose-Einstein Condensates, Phys. Rev. Lett. **123**, 015301 (2019).

[49] G. I. Martone, Y. Li, and S. Stringari, Approach for making visible and stable stripes in a spin-orbit-coupled Bose-Einstein superfluid, Phys. Rev. A **90**, 041604(R) (2014).

[50] G. Rowlands, On the stability of solutions of the non-linear Schrödinger equation, IMA J. Appl. Math. **13**, 367 (1974).

[51] N. Bottman, B. Deconinck, and M. Nivala, Elliptic solutions of the defocusing NLS equation are stable, J. Phys. A: Math. Theor. **44**, 285201 (2011).

[52] T. Gallay and D. Pelinovsky, Orbital stability in the cubic defocusing NLS equation: I. Cnoidal periodic waves, J. Differ. Equations **258**, 3607 (2015).

[53] S. Gustafson, S. Le Coz, and T.-P. Tsai, Stability of periodic waves of 1D cubic nonlinear Schrödinger equations, Appl. Math. Res. Express **2017**, 431 (2017).

[54] Y. Castin, in *Coherent Atomic Matter Waves*, edited by R. Kaiser, C. Westbrook, and F. David, *Proceedings of the Les Houches Summer School of Theoretical Physics, LXXII, 1999* (Springer, Berlin, 2001).

[55] C. J. Pethick and H. Smith, *Bose-Einstein Condensation in Dilute Gases*, 2nd ed. (Cambridge University Press, Cambridge, 2008).

[56] L. P. Pitaevskii and S. Stringari, *Bose-Einstein Condensation and Superfluidity* (Oxford University Press, Oxford, 2016).

[57] Y. Li, G. I. Martone, L. P. Pitaevskii, and S. Stringari, Superstripes and the Excitation Spectrum of a Spin-Orbit-Coupled Bose-Einstein Condensate, Phys. Rev. Lett. **110**, 235302 (2013).

[58] G. I. Martone and G. V. Shlyapnikov, Drag force and superfluidity in the supersolid stripe phase of a spin-orbit-coupled Bose-Einstein condensate, Zh. Eksp. Teor. Fiz. **154**, 985 (2018) [J. Exp. Theor. Phys. **127**, 865 (2018)].

[59] N. W. Ashcroft and N. D. Mermin, *Solid State Physics* (Saunders, Philadelphia, 1976).

[60] H. Watanabe and T. Brauner, Spontaneous breaking of continuous translational invariance, Phys. Rev. D **85**, 085010 (2012).

[61] C. Josserand, Y. Pomeau, and S. Rica, Patterns and supersolids, Eur. Phys. J. Spec. Top. **146**, 47 (2007).

[62] S. Saccani, S. Moroni, and M. Boninsegni, Excitation Spectrum of a Supersolid, Phys. Rev. Lett. **108**, 175301 (2012).

[63] M. Kunimi and Y. Kato, Mean-field and stability analyses of two-dimensional flowing soft-core bosons modeling a supersolid, Phys. Rev. B **86**, 060510(R) (2012).

[64] T. Macrì, F. Maucher, F. Cinti, and T. Pohl, Elementary excitations of ultracold soft-core bosons across the superfluid-supersolid phase transition, Phys. Rev. A **87**, 061602(R) (2013).

[65] R. Liao, Searching for Supersolidity in Ultracold Atomic Bose Condensates with Rashba Spin-Orbit Coupling, Phys. Rev. Lett. **120**, 140403 (2018).

[66] G. I. Martone, Y. Li, L. P. Pitaevskii, and S. Stringari, Anisotropic dynamics of a spin-orbit-coupled Bose-Einstein condensate, Phys. Rev. A **86**, 063621 (2012).

[67] Y. Kora and M. Boninsegni, Patterned Supersolids in Dipolar Bose Systems, J. Low Temp. Phys. **197**, 337 (2019).

[68] S. M. Roccuzzo (private communication) (unpublished).

[69] H. Watanabe and H. Murayama, Redundancies in Nambu-Goldstone Bosons, Phys. Rev. Lett. **110**, 181601 (2013).

[70] R. Onofrio, C. Raman, J. M. Vogels, J. R. Abo-Shaeer, A. P. Chikkatur, and W. Ketterle, Observation of Superfluid Flow in a Bose-Einstein Condensed Gas, Phys. Rev. Lett. **85**, 2228 (2000).

[71] N. Pavloff, Breakdown of superfluidity of an atom laser past an obstacle, Phys. Rev. A **66**, 013610 (2002).

[72] P. Engels and C. Atherton, Stationary and Nonstationary Fluid Flow of a Bose-Einstein Condensate Through a Penetrable Barrier, Phys. Rev. Lett. **99**, 160405 (2007).

[73] A. M. Leszczyszyn, G. A. El, Y. G. Gladush, and A. M. Kamchatnov, Transcritical flow of a Bose-Einstein condensate through a penetrable barrier, Phys. Rev. A **79**, 063608 (2009).

[74] D. Dries, S. E. Pollack, J. M. Hitchcock, and R. G. Hulet, Dissipative transport of a Bose-Einstein condensate, Phys. Rev. A **82**, 033603 (2010).

[75] A. M. Kamchatnov and N. Pavloff, Generation of dispersive shock waves by the flow of a Bose-Einstein condensate past a narrow obstacle, Phys. Rev. A **85**, 033603 (2012).

[76] R. Balbinot, I. Carusotto, A. Fabbri, C. Mayoral, and A. Recati, in *Analogue Gravity Phenomenology*, edited by D. Faccio, F. Belgiorno, S. Cacciatori, V. Gorini, S. Liberati, and U.

Moschella, Lecture Notes in Physics Vol. 870 (Springer, Cham, 2013).

[77] A. Coillet, I. Balakireva, R. Henriet, K. Saleh, L. Larger, J. M. Dudley, C. R. Menyuk, and Y. K. Chembo, Azimuthal Turing patterns, bright and dark cavity solitons in Kerr combs generated with whispering-gallery-mode resonators, IEEE Photon. J. **5**, 6100409 (2013).

[78] T. Herr, V. Brasch, J. D. Jost, C. Y. Wang, N. M. Kondratiev, M. L. Gorodetsky, and T. J. Kippenberg, Temporal solitons in optical microresonators, Nat. Photon. **8**, 145 (2014).

[79] J. Pfeifle, A. Coillet, R. Henriet, K. Saleh, P. Schindler, C. Weimann, W. Freude, I. V. Balakireva, L. Larger, C. Koos, and Y. K. Chembo, Optimally Coherent Kerr Combs Generated with Crystalline Whispering Gallery Mode Resonators for Ultrahigh Capacity Fiber Communications, Phys. Rev. Lett. **114**, 093902 (2015).

[80] D. C. Cole, E. S. Lamb, P. Del'Haye, S. A. Diddams, and S. B. Papp, Soliton crystals in Kerr resonators, Nat. Photon. **11**, 671 (2017).

[81] J. Petter, J. Schröder, D. Träger, and C. Denz, Optical control of arrays of photorefractive screening solitons, Opt. Lett. **28**, 438 (2003).

[82] A. S. Desyatnikov, D. N. Neshev, Y. S. Kivshar, N. Sagemerten, D. Träger, J. Jägers, C. Denz, and Y. V. Kartashov, Nonlinear photonic lattices in anisotropic nonlocal self-focusing media, Opt. Lett. **30**, 869 (2005).

[83] G. Xu, A. Chabchoub, D. E. Pelinovsky, and B. Kibler, Observation of modulation instability and rogue breathers on stationary periodic waves, Phys. Rev. Res. **2**, 033528 (2020).

[84] A. Amo, J. Lefrère, S. Pigeon, C. Adrados, C. Ciuti, I. Carusotto, R. Houdré, E. Giacobino, and A. Bramati, Superfluidity of polaritons in semiconductor microcavities, Nat. Phys. **5**, 805 (2009).

[85] E. T. Whittaker and G. N. Watson, *A Course of Modern Analysis*, 4th ed. (Cambridge University Press, Cambridge, 1996).

[86] R. G. Langebartel, Fourier expansions of rational fractions of elliptic integrals and Jacobian elliptic functions, SIAM J. Math. Anal. **11**, 506 (1980).

[87] N. S. Manton, An effective Lagrangian for solitons, Nucl. Phys. B **150**, 397 (1979).

[88] P. G. Kevrekidis, A. Khare, and A. Saxena, Solitary wave interactions in dispersive equations using Manton's approach, Phys. Rev. E **70**, 057603 (2004).

[89] M. Ishikawa and H. Takayama, Solitons in a one-dimensional Bose system with the repulsive interaction, J. Phys. Soc. Jpn. **49**, 1242 (1980).

[90] S. I. Shevchenko, On quasi-one-dimensional superfluidity in Bose systems, Fiz. Nizk. Temp. **14**, 1011 (1988) [Sov. J. Low Temp. Phys. **14**, 553 (1988)].

[91] I. V. Barashenkov and E. Y. Panova, Stability and evolution of the quiescent and traveling solitonic bubbles, Physica D **69**, 114 (1993).

[92] I. V. Barashenkov and A. O. Harin, Nonrelativistic Chern-Simons Theory for the Repulsive Bose Gas, Phys. Rev. Lett. **72**, 1575 (1994).

[93] L. P. Pitaevskii, Dynamics of solitary waves in ultracold gases in terms of observable quantities, Usp. Fiz. Nauk **186**, 1127 (2016) [Phys. Usp. **59**, 1028 (2016)].